JOURNAL OF CHEMICAL INFORMATION AND MODELING

Article

pubs.acs.org/jcim

Steered Molecular Dynamics Simulations for Studying Protein–Ligand Interaction in Cyclin-Dependent Kinase 5

Jagdish Suresh Patel,[†] Anna Berteotti,*[,†] Simone Ronsisvalle,[‡] Walter Rocchia,[†] and Andrea Cavalli*[,†,§]

[†]Department of Drug Discovery and Development, Istituto Italiano di Tecnologia, Via Morego 30, I-16163 Genova, Italy

[‡]Department of Drug Sciences, Universiy of Catania, Via A. Doria 6, I-95125 Catania, Italy

[§]Department of Pharmacy and Biotechnology, University of Bologna, Via Belmeloro 6, I-40126 Bologna, Italy

Supporting Information

ABSTRACT: In this study, we applied steered molecular dynamics (SMD) simulations to investigate the unbinding mechanism of nine inhibitors of the enzyme cyclin-dependent kinase 5 (CDK5). The study had two major objectives: (i) to create a correlation between the unbinding force profiles and the inhibition activities of these compounds expressed as IC_{50} values; (ii) to investigate the unbinding mechanism and to reveal atomistic insights, which could help identify accessory binding sites and transient interactions. Overall, we carried out 1.35 μs of cumulative SMD simulations. We showed that SMD could qualitatively discriminate binders from nonbinders, while it failed to properly rank series of inhibitors, particularly when IC_{50} values were too similar. From a mechanistic standpoint, SMD provided useful insights related to transient and dynamical interactions, which could complement static description obtained by X-ray crystallography experiments. In conclusion, the present study represents a further step toward a systematic exploitation of SMD and other dynamical approaches in structure-based drug design and computational medicinal chemistry.

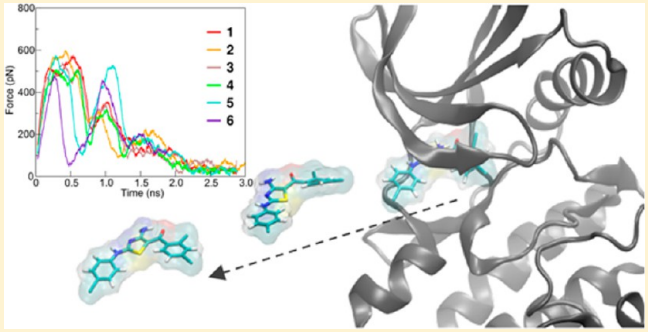

INTRODUCTION

In structure-based drug design, the estimation of drug-binding affinities remains a challenging task. This is mainly due to the high number of degrees of freedom of the overall system comprising the small molecule, its biological target, and the solvent, which hampers a proper estimation of the binding free energy.[1] Within this context, several computational approaches have recently been reported in the literature.[2−13] This is because the prediction of protein−ligand binding free energy can help in identifying hits and optimizing lead compounds, thus accelerating the discovery of new drugs.[14] Indeed, several innovative computational techniques are nowadays available to describe the process of protein−ligand recognition and binding.[9−11] Among them, steered molecular dynamics (SMD) takes inspiration from single-molecule pulling experiments[12] and forces the system to evolve away from its initial equilibrium condition, thus accelerating transitions between different energy minima.[15,16] Analyses of SMD trajectories provide atomistic information about the process under investigation. In addition, quantitative estimates of the free energy difference between two (or more) states can eventually be obtained via the Jarzynski equality.[17] SMD simulations have become very popular and are extensively applied in studying many biophysical processes, including the (un)folding mechanism of proteins,[18,19] the transportation of ions[20,21] and organic compounds through membrane channels,[22,23] and other biochemical phenomena.[24] In drug discovery, SMD is emerging as an innovative tool for gaining insights into the binding/unbinding mechanism between small molecules and their target proteins. SMD is also a promising tool for making comparisons between the rupture force and affinity of a ligand for its target protein.[14] Recently, Colizzi et al. have reported on a new SMD-based approach for discerning active from inactive inhibitors of the enzyme β-hydroxyacyl-ACP dehydratase from *Plasmodium falciparum*.[25] In particular, they computed the forces required to extract some structurally related inhibitors from the protein binding pocket and compared them to experimental data. Active inhibitors were strongly bound to the target. Steering them out of the protein binding site resulted in rupture forces higher than those observed for inactive compounds. In a subsequent study, Mai et al.[26] used SMD simulations to pull 32 ligands out of the swine A/H1N1 neuraminidase active site. Twenty-seven of the 32 molecules were marketed drugs or endogenous ligands. Interestingly, in these SMD runs, some ligands within the data set showed higher rupture forces relative to the marketed drugs, suggesting that these inhibitors could potentially be more potent than the commercial compounds. In a further study,[27] the same authors used SMD to demonstrate that R-125489 could bind to the neuraminidase more tightly than its pro-drug CS-8958, in agreement with experimental data. In the same study, the

Received: June 21, 2013
Published: January 17, 2014

dx.doi.org/10.1021/ci4003574 | J. Chem. Inf. Model. 2014, 54, 470−480

authors also proposed that R-125489 could not only bind wild-type but also Tamiflu-resistant N294S, H274Y variants of A/H5N1 virus.

In the present study, we applied SMD in the field of kinase inhibitor drug design. Unlike other targets previously investigated with SMD, kinases bear both a solvent-exposed active site and high amino acid flexibility near the binding pocket.[28] These features render SMD simulations applied to kinases particularly awkward. This study was focused on cyclin-dependent kinase 5 (CDK5), an important target for the medicinal chemistry community.[28] CDK5 is involved in the hyperphosphorylation of tau, which can lead to the formation of paired helical filaments and deposition of cytotoxic neurofibrillary tangles, one of the two histopathological hallmarks of Alzheimer's disease.[29] In addition to AD, CDK5/p25 has been implicated in cerebral ischemia, multiple sclerosis, Huntington's disease, Parkinson's disease, and amyotrophic lateral sclerosis.[30] CDK5 has also been shown to mediate the phosphorylation of the PPAR-γ receptor at specific sites, leading to insulin resistance.[31] Here, we used SMD simulations to pull two different series of inhibitors out of the CDK5 binding pocket. The inhibiting potencies (IC_{50} values) of these molecules ranged between 10^{-1} and 10^{2} μM, making the set particularly suitable for correlations between theoretical and experimental data. Multiple pulling simulations were carried out to check the performance of SMD in ranking inhibitors either intra- or interseries. As a result, we found that SMD was able to discriminate active from inactive compounds when they belonged to a congeneric series. SMD failed to properly rank ligands with very similar inhibiting potencies or those that belonged to different chemical classes. In all cases, SMD simulations provided fundamental atomistic details about the protein−ligand unbinding mechanisms, identifying transient and dynamical interactions that can be exploited for drug design purposes.

RESULTS AND DISCUSSION

CDK5 has the classical bilobal kinase fold, where the N-terminal domain (N-lobe) comprises β-sheets and one α-helix (the αC-helix), whose correct orientation is important for catalysis. The C-terminal domain (C-lobe) is mainly α-helical and is linked to the N-terminal by a flexible hinge (amino acids 81−84). Between the lobes, there is a deep cleft that natively binds ATP. The ceiling of the ATP-binding site, named the G-loop (amino acids 11 to 18), is rich in glycines and quite flexible. There is also an activation loop (T-loop), which binds the two terminal lobes (amino acids 145−165). As with other kinases, CDK5 is quite flexible and undergoes large-scale conformational motions.[32,33]

Two series of CDK5 inhibitors (see Table 1) were studied with SMD. Compounds **1**−**5** belonged to a series of 4-aminothiazole inhibitors (series I) and were used for intraseries comparisons. **6** was a virtual compound subsequently designed to further validate intraseries results (series I). Compounds **2** and **7**−**9** (series II) were ligands belonging to different chemical classes and were used for interseries comparisons. All the compounds were classical type-I kinase inhibitors,[37] that is, they were ATP competitors and bound CDK5 into the ATP binding site, interacting with the hinge region via hydrogen bonds (H-bonds) with Cys83 and Glu81. The initial pose for each CDK5−inhibitor complex was obtained from an X-ray structure, when available (compounds **2** and **7**−**9**). For the series of 4-aminothiazole derivatives (compounds **1**, **3**−**6**), the initial poses were obtained by docking simulations using the crystallographic structure of CDK5 in complex with **2** (PDB entry: 3O0G).[34] Before running SMD, 10 ns of plain MD simulations were carried out. The X-ray poses of compounds **2** and **7**−**9** as well as the docked poses of compounds **1** and **3**−**6** were stable, and 50 snapshots were randomly extracted from the last 2 ns of the MD runs, as starting poses for the subsequent SMD runs. Different possible pulling directions (see Methods), pulling velocities, spring constants, and pulling lengths were investigated (see the Supporting Information (SI) for further details). Finally, 50 independent SMD simulations, starting from 50 snapshots randomly extracted from the last 2 ns of classical MD runs were performed for each compound of both series (overall, 1.35 μs of SMD simulations) using the same pulling velocities (0.007 Å/ps) and the same pulling

Table 1. Chemical Structures and IC_{50} Values[34] of the CDK5 Inhibitors Investigated in This Study[a]

Compound	Structure	Series	IC_{50} (μM)
1	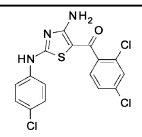	I	0.7
2	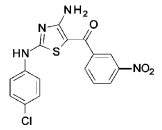	I/II	2.0
3	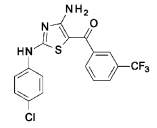	I	38
4	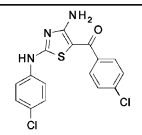	I	66
5	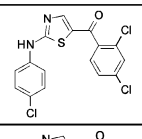	I	>100
6	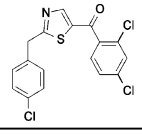	I	N/A
7	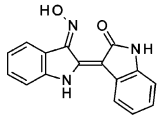	II	0.1
8	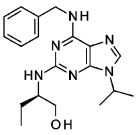	II	0.16
9	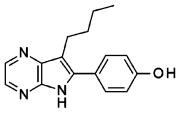	II	0.16-0.2

[a]Compounds **7**, **8**, and **9** are also known as indirubin-3′-oxime,[35] (*R*)-roscovitine,[36] and aloisine-A,[28] respectively.

dx.doi.org/10.1021/ci4003574 | J. Chem. Inf. Model. 2014, 54, 470−480

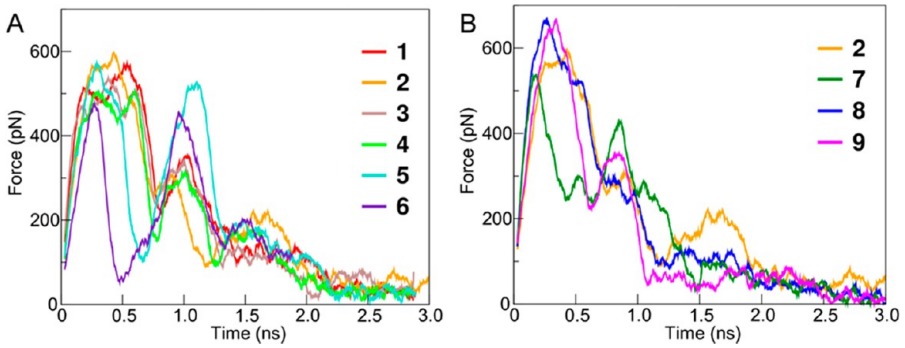

Figure 1. Average force profiles as a function of time for compounds **1**–**6** (series I, panel A) and **2** and **7**–**9** (series II, panel B).

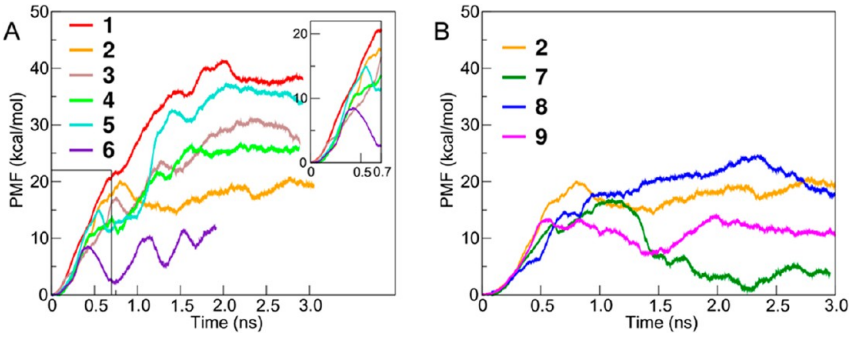

Figure 2. Potential of mean force (PMF) profiles for compounds **1**–**6** (series I). The inset plot shows a zoom view of the initial part of PMF profiles, up to 0.7 ns. The inhibiting potency order is **1** > **2** > **3** > **4** > **5** (see Table 1) and is in good agreement with the PMF profiles. In panel B, the PMF profiles for compounds **2** and **7**–**9** (series II) are shown. Conversely in this case, no correlation could be found between PMFs and experimental data.

directions. The conditions for these 50 SMD simulations are different only for the starting configuration and for the initial velocities.

Force and Potential of Mean Force (PMF) Profiles. In Figure 1A, we report the average force profiles as a function of the simulation time obtained from 50 SMD simulations for compounds **1**–**6**. At the beginning of each simulation (t = 0 ns), the ligand is in the bound state, interacting with the protein residues at the ATP binding site. After 2 ns, the ligand is completely out of the binding site and fully solvated (see the Supporting Information).

For all compounds of series I, the force profile showed two peaks: before and after 0.7 ns. The first corresponded to the rupture of the H-bonds between compounds **1**–**6** and Cys83 and Glu81. Moving further out, the ligands encountered a second barrier around 1 ns. This barrier was due to transient interactions encountered by these compounds on their way out of the binding site (see below for a mechanistic description). After 2 ns, the force approached zero, suggesting that the ligands were completely dissociated from the CDK5 binding pocket. The height of the first peak for all the ligands was about 500–600 pN; whereas the height of the second peak ranged between 300 and 500 pN. The values of the highest rupture force (before ∼ 0.7 ns) could not be used to rank the compounds. In fact, the primary rupture forces for pulling **1**–**6** out of the CDK5 binding pocket were quite similar. Conversely, the duration of the primary rupture force was fairly well correlated with the inhibition activity. The inactive compound **5** and the *bona fide* inactive molecule **6** showed decay around 0.6 and 0.5 ns, respectively, while, for the active inhibitors **1**–**4**, the decay occurred at about 0.7 ns. We could therefore conclude that, in series I, the duration of the force peaks could be used to distinguish active from inactive compounds. However, this was only a qualitative estimation, as a proper ranking of **1**–**6** in agreement with experimental IC_{50} values was not possible.

In Figure 1B, we report the average force profiles over 50 runs of SMD for the noncongeneric series of CDK5 inhibitors (series II). All the ligands showed a quite similar inhibition activity, with IC_{50} values between 0.1 and 2.0 μM (see Table 1). From the average force profiles shown in Figure 1B, we could observe that the height of the first peak was between ∼550 and ∼650 pN. From these data, it clearly emerges that SMD was unable to properly rank CDK5 inhibitors with IC_{50} values in the micromolar range. However, the different force profiles observed for each of these compounds along the unbinding pathway clearly pointed to different unbinding mechanisms (see below).

Finally, we calculated the potential of mean force (PMF) using the Jarzynski equality[38] (see the Methods section for details). Figure 2A shows the PMF profiles for compounds of series I, while Figure 2B shows the same profile for series II. For series I, the PMF profiles (at 0.7 ns corresponding to the decay of the rupture force) correlated well with the experimental IC_{50} values. For series II, however, this plot did not provide any robust correlation between PMFs and experimental IC_{50} values.

In the case of a quite broad range of inhibition activity data (series I), SMD was able to discriminate active from inactive compounds. Conversely, when IC_{50} values were similar (series II), SMD was unable to properly rank the compounds. A possible explanation for this failure could be related to the SMD pulling velocities, which should be very low to allow a proper reconstruction of accurate PMF profiles, which can then be quantitatively correlated with experimental data. However,

dx.doi.org/10.1021/ci4003574 | J. Chem. Inf. Model. 2014, 54, 470–480

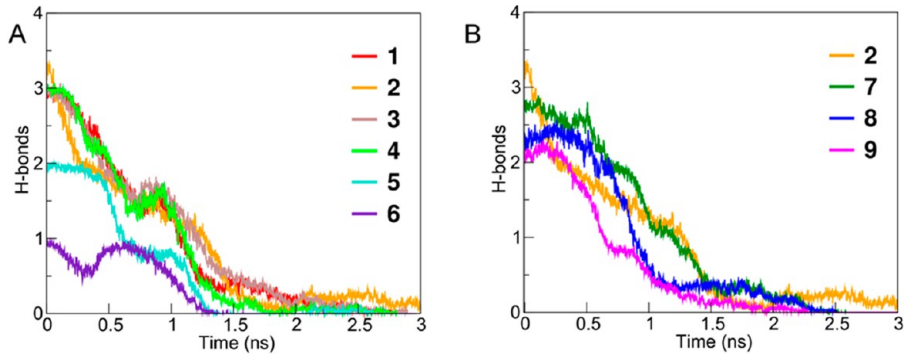

Figure 3. Total number of H-bonds established with the hinge region of the protein along the undocking process: panel A for series I, panel B for series II.

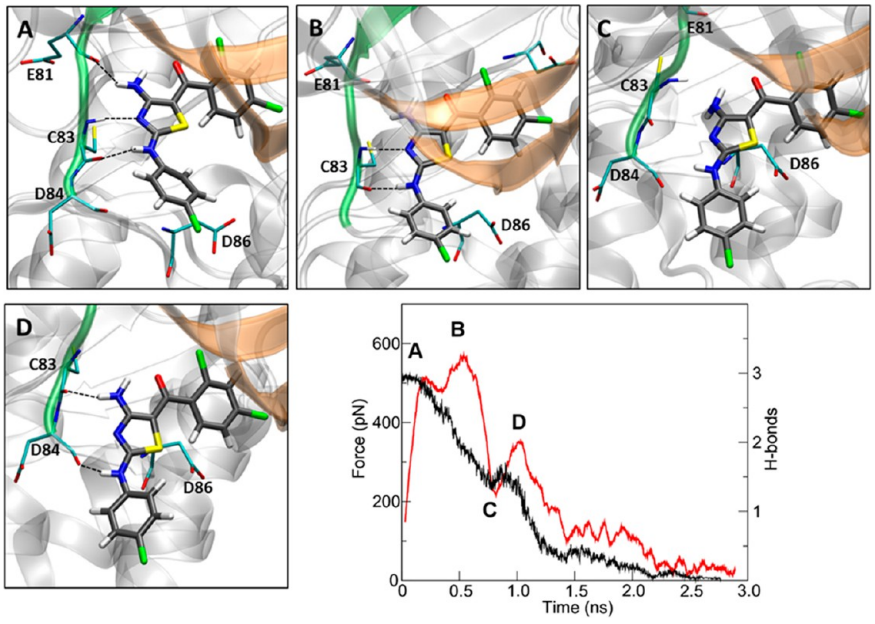

Figure 4. Mechanistic features of the undocking process of **1**. The plot represents the average force profile in red and the total number of H-bonds formed between the ligand and the protein during the unbinding event in black. Panels A, B, C, and D show the position of the ligand within the ATP binding pocket and correspond to points **A**, **B**, **C**, and **D** in the plot panel.

as mentioned, discrimination between binders and nonbinders can still be achieved using high pulling velocities, which require simulation resources in line with the drug discovery requirements of speed and cost-effectiveness. In the limit of infinite steering trajectories starting from the correct distributions of configurations, SMD is able to provide all the energetic terms of the interaction, including both enthalpic and entropic contributions. However, when SMD is used in a more restricted setting, the accuracy in the enthalpy estimation is expected to be greater than that in the entropy. This can be a reason for the partial disagreement with the experimental data, although in the present study the starting conformations for the 50 replicas of the SMD simulations for each ligand were randomly extracted from the last 2 ns of the MD runs, thus ensuring a good starting distribution of configurations.

In series I, the most significant feature for the discrimination between active and inactive compounds was the first peak decay. In addition, the estimation of PMFs also provided a good correlation between IC_{50} and PMF values.

Very few applications of SMD in drug discovery have so far been reported in the literature. In the work of Colizzi et al.,[25] from the SMD-based force profiles, the authors were able to discern active from inactive compounds against β-hydroxyacyl-ACP dehydratase of *Plasmodium falciparum*. In that case, more potent inhibitors showed higher rupture forces relative to inactive compounds. Here, for series I, the value of the highest rupture force peak was not useful for discriminating active from inactive ligands. Rather, the decay of the primary rupture force along the simulation time showed a correlation with the inhibition activity. In addition, force profiles pointed to quite different unbinding mechanisms for both series (I and II). Therefore, we focused next on the structural information that could be gained by an in-depth analysis of the SMD-generated trajectories of the unbinding mechanisms.

Unbinding Mechanisms. Insights into the nature of the unbinding mechanism come from studying the interactions between the ligand and the protein as a function of the simulated time. ATP competitors usually bind kinases establishing pivotal H-bonds, which represent the primary interactions between ligand and target. Therefore, we analyzed the interactions between CDK5 and compounds **1**−**9** in terms of total number of H-bonds (see the Supporting Information for further details). In Figure 3A, the total number of H-bonds between compounds **1**−**6** and CDK5 is plotted as a function of

dx.doi.org/10.1021/ci4003574 | J. Chem. Inf. Model. 2014, 54, 470−480

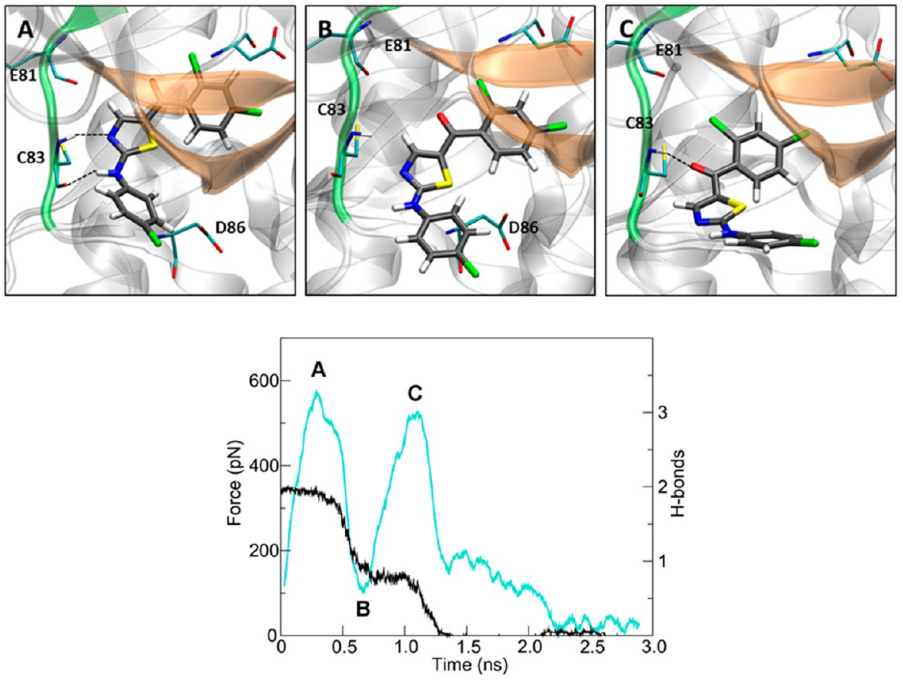

Figure 5. Unbinding mechanism of **5**, the inactive compound of series I. The plot represents the average force profile (cyan line) and the total number of H-bonds (black line) as a function of the simulation time. The letters in the plot correspond to panels A, B, and C, which show the atomistic features of the unbinding event.

time. In the bound state, compounds **1**, **3**, and **4** interacted with the protein by means of three H-bonds, while **2** established more than three H-bonds via the nitro group that interacts with Lys33. Figure 3A also shows that the three H-bonds were not broken simultaneously. Rather, this happened in a stepwise fashion. In fact, the primary rupture forces had similar values, around 500−600 pN at 0.7 ns (see Figure 1A). At time 0, compound **1** established three H-bonds with the protein. Between 0.0 and 0.5 ns, one H-bond was disrupted, and, at 0.7 ns, the other two H-bonds were finally broken. In the force profile (Figure 1A), the resulting decay of the first peak occurred around 0.7 ns. For **5** and **6**, the inactive and the *bona fide* inactive compounds, the number of H-bonds was two and one, respectively. For **5** and **6**, less time was required to break the H-bonds and a quick drop in the force intensity was observed (Figure 1A). Remarkably, the *height* of the peak (500−600 pN) was almost the same for **1**−**6**, demonstrating that the forces required to extract these compounds from the CDK5 binding pocket was mainly related to the breaking of one H-bond interaction, whereas the *length* of the peak could account for the number of H-bonds established between inhibitors and enzyme.

In Figure 3B, the total number of H-bonds established by compounds **2** and **7**−**9** with CDK5 plotted as a function of time. Compounds **8** and **9** showed a stepwise H-bond breaking pattern; whereas, for **7**, three H-bonds were kept for 0.5 ns of SMD simulations. On the basis of these observations, we next analyzed the unbinding mechanism of compounds **1** and **5** of series I and **7**−**9** of series II from CDK5.

Figure 4 shows the mechanical features of the unbinding of compound **1**. This ligand is the most potent inhibitor of series I. It showed an unbinding mechanism remarkably similar to that of **2**, **3**, and **4**. Compound **1** bound CDK5 by means of three H-bonds: (i) one between the 4-amino group of the ligand and the carbonyl oxygen Glu81 backbone; (ii) one between the nitrogen atom of the thiazole ring and the amide of Cys83 backbone; (iii) one between the 2-amino nitrogen atom and the oxygen of the Cys83 backbone (see Figure 4A). This is also reported in the plot of Figure 4, where the H-bonds and the average force profile are plotted as a function of the SMD simulation time. Pulling **1** out of the CDK5 binding pocket, the ligand first lost the H-bond with the oxygen of Glu81 backbone (see Figure 4B), and subsequently, around 0.7 ns, the other two H-bonds were also broken (see Figure 4C). This was responsible for the remarkable drop in the average force profile. However, **1** was not completely out of the binding pocket yet, as it could establish other transient interactions with either the oxygen of Cys83 backbone or Asp84. These were transient interactions, which were observed around 1 ns, and which were also evident in the plots of the H-bond patterns and the average force profiles.

Figure 5 reports the unbinding mechanism of **5**, the inactive compound of series I. At the beginning of SMD simulation, ligand **5** interacted via two H-bonds with Cys83. These interactions can also be seen from the H-bond pattern reported in the plots of Figure 5. In the absence of the 4-amino group on the thiazole ring, the pulling forces acted on the H-bonds with Cys83 backbone. The height of the force peak was similar to that observed for compounds **1**−**4**; whereas, the decay of the force was much faster. In fact, **5** lost the two H-bonds with the hinge region at around 0.6 ns (see the plot in Figure 5). Compound **5** was not completely out of the binding pocket yet, and it could still interact with the protein. In particular, the carbonyl oxygen of **5** established a strong and long spanning H-bond interaction with Cys83 backbone, which was responsible for the second peak in the force profile observed around 1 ns (see plot in Figure 5). To further validate the results obtained for series I, we designed **6**, which lacked both the 4-amino group on the thiazole ring and the amino group bridging the thiazole and the phenyl rings. **6** established a single H-bond

dx.doi.org/10.1021/ci4003574 | J. Chem. Inf. Model. 2014, 54, 470−480

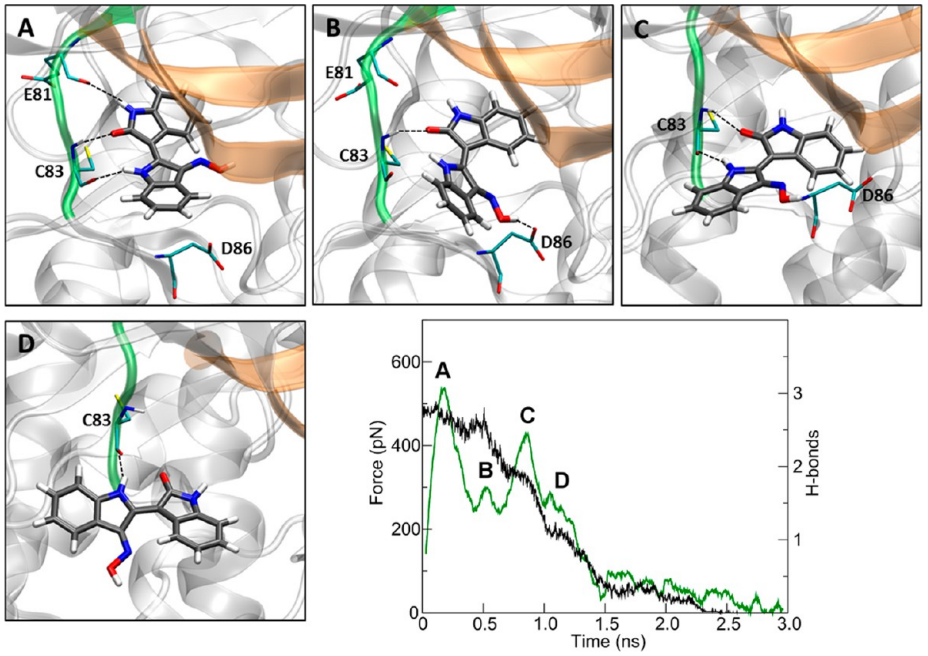

Figure 6. Mechanistic features of the undocking process of compound **7** (i.e., Indirubin). The plot represents the average force profile, in green line, and the total number of H-bonds formed between the ligand and the protein during the unbinding event. The panels A, B, C, and D show the position of the ligand within the ATP binding pocket and correspond to the points **A**, **B**, **C**, and **D** of the average force profile.

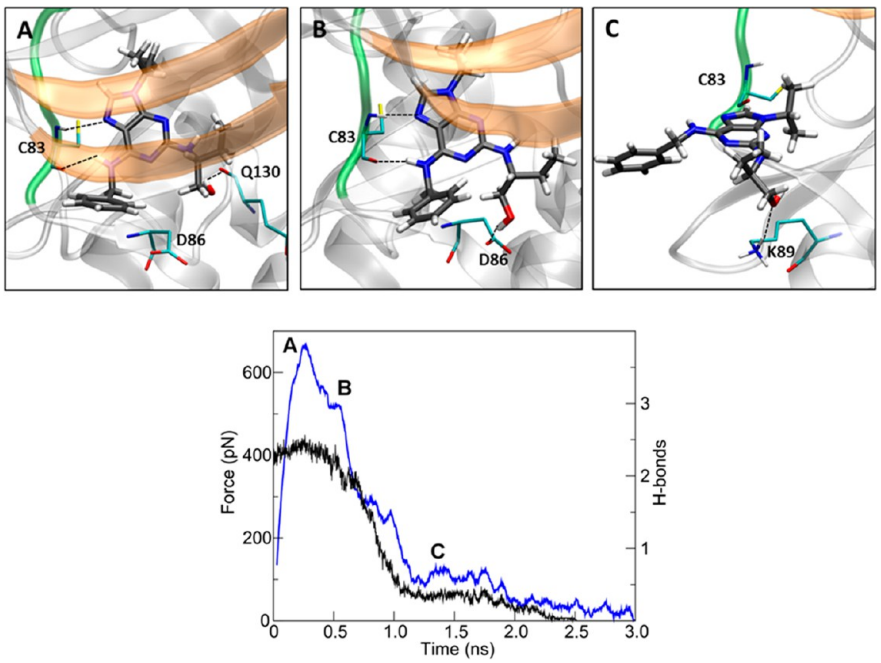

Figure 7. Unbinding mechanism of compound **8** of series II. The plot represents the average force profile (blue line) and the total number of H-bonds (black line) as a function of the simulation time. The letters in the plot correspond to panels A, B, and C, which show the atomistic features of the unbinding event.

with CDK5, which was lost (see Figure 3A) after 0.5 ns of SMD simulations (see Figure 1A). Then, the unbinding mechanism of **6** was similar to that observed for **5**.

We then focused on series II, structurally unrelated CDK5 inhibitors, for which a quite diverse mechanism of unbinding could have been hypothesized.

Figure 6 shows the unbinding mechanism of compound **7**, the most potent CDK5 inhibitor here investigated. In the crystallographic complex, **7** establishes three H-bond interactions with the amino acids of the hinge region, Glu81 and Cys83 (see Figure 6A and B). Applying pulling forces, **7** quickly lost the interactions with Glu81 and Cys83, generating a sharp peak, as observed in the force profile (see the plot in Figure 6). At 0.5 ns, the ligand still maintained one H-bond with the hinge region, while the rest of the molecule was bent in such a way as to allow its hydroxyl group to interact with the carboxylate of Asp86 (see Figures 6B). This was a temporary interaction that was immediately lost, leading **7** back to its original position,

dx.doi.org/10.1021/ci4003574 | J. Chem. Inf. Model. 2014, 54, 470−480

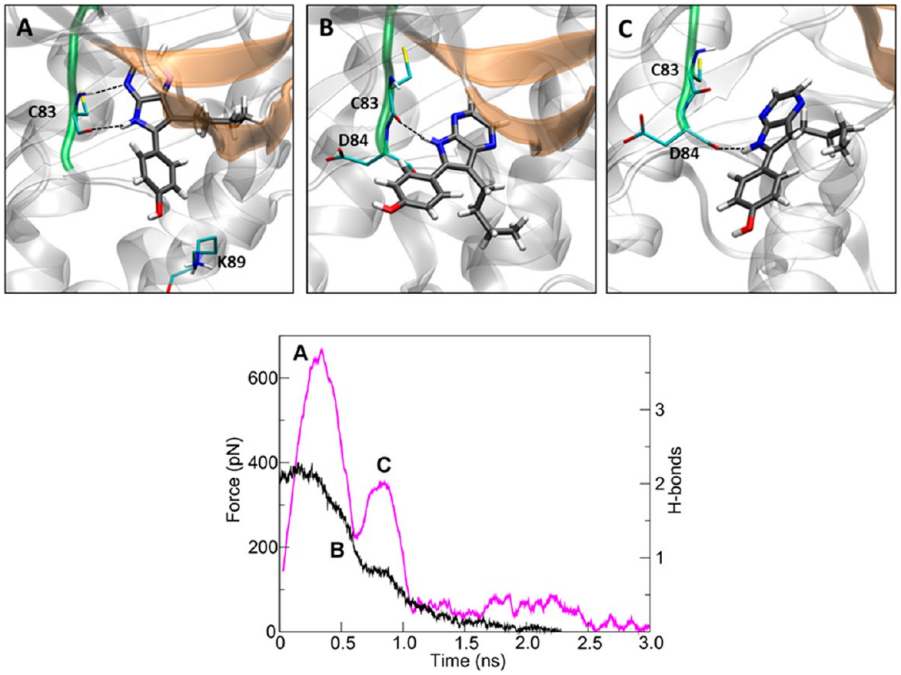

Figure 8. Unbinding mechanism of compound **9**. The plot represents the average force profile (magenta line) and the total number of H-bonds (black line) as a function of the simulation time. The letters in the plot correspond to panels A, B, and C, which show the atomistic features of the unbinding event.

where it could re-establish H-bonds with Cys83 backbone atoms (see Figures 6C). The second small peak in the force profile (see the plot in Figure 6) was related to the forces required to bring the compound from the conformation reported in Figure 6B to the conformation shown in Figure 6C. Compound **7** then lost the H-bond between its carbonyl group and the backbone of Cys83 (Figure 6D), still maintaining the second H-bond with the oxygen of Cys83 backbone. This pivotal interaction allowed the ligand to freely move at the CDK5 binding pocket around this H-bond, which was subsequently lost at about 1.6 ns, generating a fourth peak in the force profile. Interestingly, the transient interaction between the hydroxyl group of **7** and the carboxylate of Asp86, which was not observed in the crystallographic complex, can be exploited to design an analog of **7** with improved potency against CDK5.

Compound **8** in its crystallographic pose establishes two H-bonds with the hinge region residue Cys83 and with the oxygen of Gln130 backbone (Figure 7A). The latter interaction was quite weak, and it was already lost during initial MD simulations. Applying a pulling force with SMD simulations, the H-bonds with the hinge region were broken, generating a sharp peak in the force profile. These interactions were quite persistent, as shown by the extent of the peak (see Figures 1B and 3B). Occasionally, the hydroxyl group of **8** could form an H-bond with the carboxylate of Asp86 (see Figure 7B and the plot in Figure 7). Once the ligand was out of the binding pocket, it could still maintain some residual interactions with Lys89 (Figure 7C).

The very common H-bond interactions with the Cys83 backbone atoms are also present in the crystallographic complex between CDK5 and **9** (Figure 8A). Applying SMD-based forces to this system, **9** either lost the two H-bonds with the hinge region and formed a new H-bond with the backbone oxygen of Asp84, or lost only one of the initial H-bonds, while maintaining the other (see Figure 8B and C). In the force profile related to the unbinding of **9** (see the plots in Figure 8), the first peak was due to the rupture force required to break the interactions with the hinge region, while the second peak was related to the forces required to break a single intermediate interaction with the hinge region, the H-bond between the ligand and the carbonyl group of Asp84.

A comment may be required on the ability of SMD to discriminate ligands that interact with biological targets either by means of hydrophobic or electrostatic interactions. Considering the nature of the approach, here we have shown that SMD could be more suited to identify and account for stronger and localized interactions such as H-bonds and salt bridges rather than for more spread hydrophobic interactions. Furthermore, the latter ones may involve rearrangement phenomena, which are less likely to be captured by SMD, particularly when a limited number of SMD trajectories are considered.

■ CONCLUSIONS

SMD is emerging as a promising tool in structure-based drug design. These kinds of simulations can provide two major outcomes: (i) a force (or PMF) profile which can be qualitatively and possibly quantitatively correlated with protein−ligand binding affinities; (ii) a detailed atomistic description of the unbinding mechanism of a drug out of the protein binding pocket. In this study, we performed SMD simulations using two series of CDK5 inhibitors, aimed at addressing the extent to which this tool could be used in a predictive fashion. While the approach could discriminate binders from nonbinders quite well, it failed to properly rank a series of inhibitors with similar potencies. A possible explanation for this limit could be related to the SMD pulling velocities, which should be very low to allow a proper reconstruction of accurate PMF profiles, which can then be

dx.doi.org/10.1021/ci4003574 | J. Chem. Inf. Model. 2014, 54, 470−480

quantitatively correlated with experimental data. However, as mentioned, discrimination between binders and nonbinders can still be achieved using high pulling velocities, which require simulation resources in line with the drug discovery requirements of speed and cost-effectiveness. One can therefore envision a scenario in which SMD complements much faster approaches, such as virtual ligand screening, to obtain more accurate results during hit identification. As per the mechanistic description, SMD can provide atomistic details of the unbinding mechanisms, revealing transient interactions that can be exploited in-depth for drug design. In fact, accessory binding sites are seldom revealed by X-ray experiments. In this respect, SMD can complement the fundamental information of X-ray studies, pointing to temporary interactions at accessory binding sites, which can be detected only by dynamical simulations. In conclusion, thanks to the rapid increase of CPU resources and the availability of SMD in most academic and commercial software, this approach could become a standard methodology in the hit identification step of a drug discovery project.

METHODS

Model Building and Docking Simulations. The initial 3D coordinates for the CDK5-inhibitors complexes were retrieved, if available, from the Protein Data Bank (PDB). In particular, the starting structure for the complexes of (*R*)-roscovitine, aloisine-A, and indirubin-3′-oxime with CDK5 were taken from 1UNL, 1UNG, and 1UNH[28] PDB structures, respectively. As per the congeneric series of 4-aminothiazole, we used for **2** the X-ray structure of the complex (PDB id 3O0G[34]), while the other congeneric ligands were docked to the same protein conformation. In all of the complexes, the activator p25 was removed from the crystal structure, the Asn144 was computationally mutated back to the wild-type aspartate and missing residues were built using MODELER v9.7,[39] when needed. We used the Glide v5.7 from the Schrödinger's Suite[40,41] for the docking of all the congeneric molecules of series I to the CDK5 protein. The protein receptor (PDB id 3O0G) was imported in Maestro,[42] then processed with the preparation wizard tool: all water molecules were removed and hydrogen atoms were added. The grid was centered on the geometric center of the active site residues. The size of the grid was set to 10 Å in each of the three directions and the OPLS_2005 force field[43] was used. During the docking run, default input parameters were used: no scaling factor for the van der Waals radii of nonpolar protein atoms was applied while a scaling factor of 0.8 was used for nonpolar ligand atoms with an absolute value of the partial atomic charge less than or equal to 0.15. All compounds of series I were docked and scored using the Glide extra precision (XP) mode. To assess the validity of our docking procedure, the cocrystallized compound (i.e., **2**) was subjected to the same docking protocol. We evaluated the docking pose compared to the crystallographic one, and the result was consistent. For all of the other ligands, the obtained docked poses showed binding interactions consistent with literature data.

Molecular Dynamics (MD). All the complexes were placed in an orthorhombic periodic box with a separation margin from the solute of 12 Å in each dimension by means of the LEaP program.[44] The electroneutrality of the system was achieved by adding one Cl^- ion. The following parameters, minimization, and thermalization procedures were adopted for all the complexes. Long-range electrostatic interactions were treated with the Particle Mesh Ewald (PME) method,[45] while the short-range nonbonded interactions were calculated using a cutoff radius of 10 Å for both Coulomb and van der Waals potentials with a switching function starting at 8 Å. All bond lengths involving hydrogen atoms were constrained using the SHAKE algorithm.[46] A 2 fs time integration step was used in all the simulations. A steepest-descent minimization scheme was initially applied to the system, which was then gradually heated up to 300 K by applying decreasing harmonic restraining forces in three stages. During the first stage of the thermalization, the system was heated up to 100 K in 50 ps by applying harmonic restraints with force constant of 30 kcal/mol·Å^2 on Cα atoms and 10 kcal/mol·Å^2 on C and N atoms of the protein backbone. In the second stage, the system was simulated for 100 ps by increasing the temperature up to 200 K with a force constant of 20 kcal/mol·Å^2 on Cα atoms and 5 kcal/mol·Å^2 on C and N atoms of the protein backbone. In the last stage, the temperature of the system was brought up to the desired value of 300 K after simulating for 200 ps by keeping weak harmonic restraints with a force constant of 10 kcal/mol·Å^2 on Cα atoms and of 2.5 kcal/mol·Å^2 on C and N atoms of the protein backbone. The temperature was kept constant at 300 K by the Langevin thermostat with a collision coefficient of 5 ps^{-1}. The thermalization phase (NVT ensemble) was followed by a pressurization phase (NPT ensemble), which was carried out at 1 atm pressure and 300 K by putting soft harmonic restraints only for an initial short period of time. In particular, for the first 100 ps, there were weak harmonic restraints with force constant of 5 kcal/mol·Å^2 on Cα atoms and 1.25 kcal/mol·Å^2 on C and N atoms. In the second stage of 200 ps, only Cα atoms of the protein were restrained with a force constant of 2.5 kcal/mol·Å^2. A pressure of 1 atm was maintained using the Langevin piston barostat. The system was then evolved for a further 10 ns without any restraint under NPT conditions, and the starting conformations for SMD simulations were randomly drawn from the last 2 ns of trajectory. All molecular dynamics (MD) calculations were performed with the NAMD2.8 code.[47] We used the Amber99 SB-ILDN[48] force field for the protein and the TIP3P model[49] for all water molecules of the system.

The ligands were treated with the general AMBER force field (GAFF)[50,51] for organic molecules. The corresponding topology and parameters files were prepared using the antechamber tool of the AMBER suite of programs.[44] The charges of the ligands were derived using the restrained electrostatic potential (RESP) fitting procedure[52] based on the electrostatic potential calculated with the Gaussian09[53] package using a 6-31G(d) basis set at the Hartree−Fock level of theory.

Steered Molecular Dynamics (SMD). In SMD simulations, a time-dependent external force is applied to the ligand to facilitate its unbinding from the protein, which cannot usually be achieved by standard MD simulation. In particular, in SMD, the transition between two states, here the bound and unbound ones, is achieved by adding to the standard Hamiltonian a harmonic time-dependent potential acting on a descriptor, for example the protein−ligand distance. During the transition, we can calculate the exerted force as well as the external work performed on the system (see the SI for further details).

All the SMD simulations were performed using the PLUMED[54] plugin integrated in the NAMD 2.8[47] MD code. Since we were interested in the unbinding of the ligand from the protein, the natural choice of the pulling variable was the

dx.doi.org/10.1021/ci4003574 | J. Chem. Inf. Model. 2014, 54, 470−480

distance between the protein and the ligand. In order to avoid any distortions of the protein as a consequence of pulling, the distance was defined between the center of mass of several heavy atoms of a stable part of the protein and the center of mass of selected atoms of the ligand (see the SI). The pulling parameters were adopted from Patel et al.[55] In particular, the spring constant was set to the value of 100 kcal/mol·Å^2 and the pulling velocity to 0.007 Å/ps. Finally, the maximum pulling length was chosen to be 25 Å, which ensured the complete solvation of the ligand while it was outside the binding pocket. Concerning the unbinding pathway, in our previous work[55] we identified two unbinding patterns for (*R*)-roscovitine from the CDK5 binding site. In the first path, the ligand starting from the bound pose goes in the bulk solvent by making several interactions with the hinge region. In the second path, the ligand interacts with the glycine-rich loop. However, the probability of this latter unbinding path was lower than that of the first. During trial SMD simulations, we observed that the ligands had the tendency to roll on the surface of the protein once they were out of the binding pocket, which resulted in noisy force profiles.

Therefore, we used a cylindrical harmonic restraint, which hindered the interaction of the ligand with the surface of the protein while the former was out of the binding site. This restraint was implemented as the distance of a point to the axis of the cylinder. The point was the center of mass of selected atoms of the ligand, while the axis was formed by the center of mass of two atom groups of the protein. One of these two groups was the same as that used to define the force that pulled the ligand out of the binding pocket. A harmonic restraint was applied to the upper value of this variable (in our case 5 Å). The restraint was imposed in such a way as to avoid interference with the exploration of all the possible conformations within the binding pocket. Moreover, the restraining potential only affected the center of mass of the ligand. The effect of the cylindrical restraint applied during the steering had no effect on our comparative study, as the same constraint was applied to all the systems in the very same fashion. Moreover, it does not affect the considerations on the first force peaks seen during steering as the constraint is not acting when protein and ligand are in so close contact.

The time length for each simulation was 3 ns, which was sufficient to observe the entire ligand unbinding process. The mean force profile and PMF for each ligand were calculated by averaging the outcomes of 50 independent runs.

■ ASSOCIATED CONTENT

Ⓢ Supporting Information

Details related to the Methods section; ligand solvation as a function of SMD simulation time; computational details about the total number of H-bonds; stability of the binding poses during the MD simulation. This material is available free of charge via the Internet at http://pubs.acs.org.

■ AUTHOR INFORMATION

Corresponding Authors

*A.B. Phone/Fax: +39 01071781573/228. E-mail: anna.berteotti@iit.it.

*A.C. Phone/Fax: +39 01071781530/228. E-mail: andrea.cavalli@iit.it.

Notes

The authors declare no competing financial interest.

■ ACKNOWLEDGMENTS

The Authors gratefully acknowledge the IIT platform "Computation", the DEISA project "Improving ligand binding free energy estimation through enhanced sampling algorithms" (acronym: FREESA 2010/2011), and the PRACE fifth Regular Call project (2012). The authors are also grateful to Giovanni Bottegoni, Francesco Colizzi, and Roberto Gaspari for useful discussions. The authors thank Grace Fox for editing and proofreading the manuscript.

■ ABBREVIATIONS

MD, molecular dynamics; SMD, steered molecular dynamics; CDK5, cyclin dependent kinase 5; PMF, potential of mean force; PDB, Protein Data Bank; PME, particle mesh Ewald; GAFF, generalized Amber force field

■ REFERENCES

(1) Gilson, M. K.; Zhou, H. X. Calculation of protein-ligand binding affinities. *Annu. Rev. Biophys. Biomol. Struct.* **2007**, *36*, 21−42.

(2) Shoichet, B. K.; McGovern, S. L.; Wei, B.; Irwin, J. J. Lead discovery using molecular docking. *Curr. Opin. Chem. Biol.* **2002**, *6*, 439−446.

(3) Taylor, R. D.; Jewsbury, P. J.; Essex, J. W. A review of protein-small molecule docking methods. *J. Comput. Aided Mol. Des.* **2002**, *16*, 151−166.

(4) Aqvist, J.; Medina, C.; Samuelsson, J.-E. A new method for predicting binding affinity in computer-aided drug design. *Protein Eng.* **1994**, *7*, 385−391.

(5) Srinivasan, J.; Cheatham, T. E.; Cieplak, P.; Kollman, P. A.; Case, D. A. Continuum Solvent Studies of the Stability of DNA, RNA, and Phosphoramidate-DNA Helices. *J. Am. Chem. Soc.* **1998**, *120*, 9401−9409.

(6) Qiu, D.; Shenkin, P. S.; Hollinger, F. P.; Still, W. C. The GB/SA Continuum Model for Solvation. A Fast Analytical Method for the Calculation of Approximate Born Radii. *J. Phys. Chem. A* **1997**, *101*, 3005−3014.

(7) Jorgensen, W. L.; Buckner, J. K.; Boudon, S.; Tirado-Rives, J. Efficient computation of absolute free energies of binding by computer simulations. Application to the methane dimer in water. *J. Chem. Phys.* **1988**, *89*, 3742−3746.

(8) Gilson, M.; Given, J.; Bush, B.; McCammon, J. The statistical-thermodynamic basis for computation of binding affinities: a critical review. *Biophys. J.* **1997**, *72*, 1047−1069.

(9) Pietrucci, F.; Marinelli, F.; Carloni, P.; Laio, A. Substrate binding mechanism of HIV-1 protease from explicit-solvent atomistic simulations. *J. Am. Chem. Soc.* **2009**, *131*, 11811−11818.

(10) Torrie, G. M.; Valleau, J. P. Nonphysical sampling distributions in Monte Carlo free-energy estimation: Umbrella sampling. *J. Comput. Phys.* **1977**, *23*, 187−199.

(11) Laio, A.; Parrinello, M. Escaping Free Energy Minima. *Proc. Natl. Acad. Sci. U.S.A.* **2002**, *20*, 12562−12566.

(12) Grubmuller, H.; Heymann, B.; Tavan, P. Ligand Binding: Molecular Mechanics Calculation of the Streptavidin-Biotin Rupture Force. *Science* **1996**, *271*, 997−999.

(13) Kirkwood, J. G. Statistical Mechanics of Fluid Mixtures. *J. Chem. Phys.* **1935**, *3*, 300−313.

(14) Jorgensen, W. L. Drug discovery: Pulled from a protein's embrace. *Nature* **2010**, *466*, 42−43.

(15) Park, S.; Schulten, K. Calculating potentials of mean force from steered molecular dynamics simulations. *J. Chem. Phys.* **2004**, *120*, 5946−5961.

(16) Li, M. S.; Mai, B. K. Steered Molecular Dynamics-A Promising Tool for Drug Design. *Curr. Bioinform.* **2012**, *7*, 342−351.

(17) Park, S.; Khalili-Araghi, F.; Tajkhorshid, E.; Schulten, K. Free energy calculation from steered molecular dynamics simulations using Jarzynski's equality. *J. Chem. Phys.* **2003**, *119*, 3559−3566.

(18) Isralewitz, B.; Baudry, J.; Gullingsrud, J.; Kosztin, D.; Schulten, K. Steered molecular dynamics investigations of protein function. *J. Mol. Graphics Modell.* **2001**, *19*, 13−25.
(19) Lu, H.; Isralewitz, B.; Krammer, A.; Vogel, V.; Schulten, K. Unfolding of titin immunoglobulin domains by steered molecular dynamics simulation. *Biophys. J.* **1998**, *75*, 662−671.
(20) Giorgino, T.; De Fabritiis, G. A High-Throughput Steered Molecular Dynamics Study on the Free Energy Profile of Ion Permeation through Gramicidin A. *J. Chem. Theory Comput.* **2011**, *7*, 1943−1950.
(21) Gwan, J. F.; Baumgaertner, A. Cooperative transport in a potassium ion channel. *J. Chem. Phys.* **2007**, *127*, 045103.
(22) Henin, J.; Tajkhorshid, E.; Schulten, K.; Chipot, C. Diffusion of glycerol through Escherichia coli aquaglyceroporin GlpF. *Biophys. J.* **2008**, *94*, 832−839.
(23) Jensen, M. O.; Park, S.; Tajkhorshid, E.; Schulten, K. Energetics of glycerol conduction through aquaglyceroporin GlpF. *Proc. Natl. Acad. Sci. U.S.A.* **2002**, *99*, 6731−6736.
(24) Xu, Y.; Shen, J.; Luo, X.; Silman, I.; Sussman, J. L.; Chen, K.; Jiang, H. How does huperzine A enter and leave the binding gorge of acetylcholinesterase? Steered molecular dynamics simulations. *J. Am. Chem. Soc.* **2003**, *125*, 11340−11349.
(25) Colizzi, F.; Perozzo, R.; Scapozza, L.; Recanatini, M.; Cavalli, A. Single-molecule pulling simulations can discern active from inactive enzyme inhibitors. *J. Am. Chem. Soc.* **2010**, *132*, 7361−7371.
(26) Mai, B. K.; Viet, M. H.; Li, M. S. Top leads for swine influenza A/H1N1 virus revealed by steered molecular dynamics approach. *J. Chem. Inf. Model.* **2010**, *50*, 2236−2247.
(27) Mai, B. K.; Li, M. S. Neuraminidase inhibitor R-125489−a promising drug for treating influenza virus: steered molecular dynamics approach. *Biochem. Biophys. Res. Commun.* **2011**, *410*, 688−691.
(28) Mapelli, M.; Massimiliano, L.; Crovace, C.; Seeliger, M. A.; Tsai, L. H.; Meijer, L.; Musacchio, A. Mechanism of CDK5/p25 binding by CDK inhibitors. *J. Med. Chem.* **2005**, *48*, 671−679.
(29) Cheung, Z. H.; Ip, N. Y. Cdk5: a multifaceted kinase in neurodegenerative diseases. *Trends Cell Biol.* **2012**, *22*, 169−175.
(30) Keeney, J. T. R.; Swomley, A. M.; Harris, J. L.; Fiorini, A.; Mitov, M. I.; Perluigi, M.; Sultana, R.; Butterfield, D. A. Cell Cycle Proteins in Brain in Mild Cognitive Impairment: Insights into Progression to Alzheimer Disease. *Neurotox. Res.* **2012**, *22*, 220−230.
(31) Kim, E.; Chen, F.; Wang, C. C.; Harrison, L. E. CDK5 is a novel regulatory protein in PPARgamma ligand-induced antiproliferation. *Int. J. Oncol.* **2006**, *28*, 191−194.
(32) Morgan, D. O. Principles of CDK regulation. *Nature* **1995**, *374*, 131−134.
(33) Berteotti, A.; Cavalli, A.; Branduardi, D.; Gervasio, F. L.; Recanatini, M.; Parrinello, M. Protein conformational transitions: the closure mechanism of a kinase explored by atomistic simulations. *J. Am. Chem. Soc.* **2009**, *131*, 244−250.
(34) Ahn, J. S.; Radhakrishnan, M. L.; Mapelli, M.; Choi, S.; Tidor, B.; Cuny, G. D.; Musacchio, A.; Yeh, L. A.; Kosik, K. S. Defining Cdk5 ligand chemical space with small molecule inhibitors of tau phosphorylation. *Chem. Biol.* **2005**, *12*, 811−823.
(35) Leclerc, S.; Garnier, M.; Hoessel, R.; Marko, D.; Bibb, J. A.; Snyder, G. L.; Greengard, P.; Biernat, J.; Wu, Y. Z.; Mandelkow, E. M.; Eisenbrand, G.; Meijer, L. Indirubins inhibit glycogen synthase kinase-3 beta and CDK5/p25, two protein kinases involved in abnormal tau phosphorylation in Alzheimer's disease. A property common to most cyclin-dependent kinase inhibitors? *J. Biol. Chem.* **2001**, *276*, 251−60.
(36) Jain, P.; Flaherty, P. T.; Yi, S.; Chopra, I.; Bleasdell, G.; Lipay, J.; Ferandin, Y.; Meijer, L.; Madura, J. D. Design, synthesis, and testing of an 6-O-linked series of benzimidazole based inhibitors of CDK5/p25. *Bioorg. Med. Chem.* **2011**, *19*, 359−373.
(37) Rabiller, M.; Getlik, M.; Kluter, S.; Richters, A.; Tuckmantel, S.; Simard, J. R.; Rauh, D. Proteus in the world of proteins: conformational changes in protein kinases. *Arch. Pharm. (Weinheim)* **2010**, *343*, 193−206.
(38) Xiong, H.; Crespo, A.; Marti, M.; Estrin, D.; Roitberg, A. E. Free energy calculations with non-equilibrium methods: applications of the Jarzynski relationship. *Theor. Chem. Acc.* **2006**, *116*, 338−346.
(39) Sali, A.; Blundell, T. L. Comparative protein modelling by satisfaction of spatial restraints. *J. Mol. Biol.* **1993**, *234*, 779−815.
(40) Friesner, R. A.; Banks, J. L.; Murphy, R. B.; Halgren, T. A.; Klicic, J. J.; Mainz, D. T.; Repasky, M. P.; Knoll, E. H.; Shelley, M.; Perry, J. K.; Shaw, D. E.; Francis, P.; Shenkin, P. S. Glide: a new approach for rapid, accurate docking and scoring. 1. Method and assessment of docking accuracy. *J. Med. Chem.* **2004**, *47*, 1739−1749.
(41) Friesner, R. A.; Murphy, R. B.; Repasky, M. P.; Frye, L. L.; Greenwood, J. R.; Halgren, T. A.; Sanschagrin, P. C.; Mainz, D. T. Extra precision glide: docking and scoring incorporating a model of hydrophobic enclosure for protein-ligand complexes. *J. Med. Chem.* **2006**, *49*, 6177−6196.
(42) Seeber, M.; Cecchini, M.; Rao, F.; Settanni, G.; Caflisch, A. Wordom: a program for efficient analysis of molecular dynamics simulations. *Bioinformatics* **2007**, *23*, 2625−2627.
(43) Banks, J. L.; Beard, H. S.; Cao, Y.; Cho, A. E.; Damm, W.; Farid, R.; Felts, A. K.; Halgren, T. A.; Mainz, D. T.; Maple, J. R.; Murphy, R.; Philipp, D. M.; Repasky, M. P.; Zhang, L. Y.; Berne, B. J.; Friesner, R. A.; Gallicchio, E.; Levy, R. M. Integrated Modeling Program, Applied Chemical Theory (IMPACT). *J. Comput. Chem.* **2005**, *26*, 1752−1780.
(44) Case, D. A.; Cheatham, T. E., 3rd; Darden, T.; Gohlke, H.; Luo, R.; Merz, K. M., Jr.; Onufriev, A.; Simmerling, C.; Wang, B.; Woods, R. J. The Amber biomolecular simulation programs. *J. Comput. Chem.* **2005**, *26*, 1668−1688.
(45) Darden, T.; York, D.; Pedersen, L. Particle mesh Ewald: An N log(N) method for Ewald sums in large systems. *J. Chem. Phys.* **1993**, *98*, 10089−10092.
(46) Ryckaert, J.-P.; Ciccotti, G.; Berendsen, H. J. C. Numerical integration of the cartesian equations of motion of a system with constraints: molecular dynamics of n-alkanes. *J. Comput. Phys.* **1977**, *23*, 327−341.
(47) Phillips, J. C.; Braun, R.; Wang, W.; Gumbart, J.; Tajkhorshid, E.; Villa, E.; Chipot, C.; Skeel, R. D.; Kale, L.; Schulten, K. Scalable molecular dynamics with NAMD. *J. Comput. Chem.* **2005**, *26*, 1781−1802.
(48) Lindorff-Larsen, K.; Piana, S.; Palmo, K.; Maragakis, P.; Klepeis, J. L.; Dror, R. O.; Shaw, D. E. Improved side-chain torsion potentials for the Amber ff99SB protein force field. *Proteins* **2010**, *78*, 1950−1958.
(49) Jorgensen, W. L.; Chandrasekhar, J.; Madura, J. D.; Impey, R. W.; Klein, M. L. Comparison of simple potential functions for simulating liquid water. *J. Chem. Phys.* **1983**, *79*, 926−935.
(50) Wang, J.; Wang, W.; Kollman, P. A.; Case, D. A. Automatic atom type and bond type perception in molecular mechanical calculations. *J. Mol. Graphics Modell.* **2006**, *25*, 247−260.
(51) Wang, J.; Wolf, R. M.; Caldwell, J. W.; Kollman, P. A.; Case, D. A. Development and testing of a general amber force field. *J. Comput. Chem.* **2004**, *25*, 1157−1174.
(52) Cornell, W. D.; Cieplak, P.; Bayly, C. I.; Kollman, P. A. Application of RESP charges to calculate conformational energies, hydrogen bond energies, and free energies of solvation. *J. Am. Chem. Soc.* **1993**, *115*, 9620−9631.
(53) Frisch, M. J.; Trucks, G. W.; Schlegel, H. B.; Scuseria, G. E.; Robb, M. A.; Cheeseman, J. R.; Scalmani, G.; Barone, V.; Mennucci, B.; Petersson, G. A.; Nakatsuji, H.; Caricato, M.; Li, X.; Hratchian, H. P.; Izmaylov, A. F.; Bloino, J.; Zheng, G.; Sonnenberg, J. L.; Hada, M.; Ehara, M.; Toyota, K.; Fukuda, R.; Hasegawa, J.; Ishida, M.; Nakajima, T.; Honda, Y.; Kitao, O.; Nakai, H.; Vreven, T.; Montgomery, J. A., Jr.; Peralta, J. E.; Ogliaro, F.; Bearpark, M.; Heyd, J. J.; Brothers, E.; Kudin, K. N.; Staroverov, V. N.; Kobayashi, R.; Normand, J.; Raghavachari, K.; Rendell, A.; Burant, J. C.; Iyengar, S. S.; Tomasi, J.; Cossi, M.; Rega, N.; Millam, N. J.; Klene, M.; Knox, J. E.; Cross, J. B.; Bakken, V.; Adamo, C.; Jaramillo, J.; Gomperts, R.; Stratmann, R. E.; Yazyev, O.; Austin, A. J.; Cammi, R.; Pomelli, C.; Ochterski, J. W.; Martin, R. L.; Morokuma, K.; Zakrzewski, V. G.; Voth, G. A.; Salvador, P.; Dannenberg, J. J.; Dapprich, S.; Daniels, A. D.; Farkas, O.;

Foresman, J. B.; Ortiz, J. V.; Cioslowski, J.; Fox, D. J. *Gaussian 09*, revision A.2; Gaussian, Inc.: Wallingford, CT, 2009.
(54) Bonomi, M.; Branduardi, D.; Bussi, G.; Camilloni, C.; Provasi, D.; Raiteri, P.; Donadio, D.; Marinelli, F.; Pietrucci, F.; Broglia, R. A.; Parrinello, M. PLUMED: A portable plugin for free-energy calculations with molecular dynamics. *Comput. Phys. Commun.* **2009**, *180*, 1961−1972.
(55) Patel, J. S.; Branduardi, D.; Masetti, M.; Rocchia, W.; Cavalli, A. Insights into Ligand-Protein Binding from Local Mechanical Response. *J. Chem. Theory Comput.* **2011**, *7*, 3368−3378.